Electronic Research Archive

https://www.aimspress.com/journal/era

ERA, 34(3): 1546–1558.
DOI: 10.3934/era.2026070
Received: 25 December 2025
Revised: 04 February 2026
Accepted: 11 February 2026
Published: 13 February 2026

Research article

Prespecified-time sliding mode control for stability of maglev train suspension systems

Lingling Zhang*

School of Mathematics, Changsha University, Changsha 410022, China

* **Correspondence:** Email: z002005@163.com.

Abstract: This paper focuses on achieving prespecified-time stability in maglev suspension systems. Within a sliding mode control framework, we design three types of controllers for finite-time, fixed-time, and prespecified-time convergence. Pole assignment techniques are utilized to precisely tailor the system dynamics on the sliding manifold. The theoretical findings are validated through numerical simulations, which highlight the practical benefits of the proposed control strategies.

Keywords: maglev train; prespecified-time stability; Lyapunov approach; sliding mode control

1. Introduction

Maglev trains are classified into two main types: electrodynamic suspension (EDS) and electromagnetic suspension (EMS) systems [1]. EDS trains employ superconducting magnets to generate repulsive forces, achieving stable levitation at gaps exceeding 10 mm and enabling high-speed operation. However, they require a minimum velocity to initiate lift-off [2]. In contrast, EMS trains utilize electromagnetic attraction for levitation, even at zero speed, though their inherent instability demands active control to maintain a consistent air gap (approximately 10 mm) [3–5]. This requirement makes EMS systems a prominent research area in control engineering. Given the maturity of EMS-type maglev technology, most national maglev initiatives adopt this approach-including the study presented in this paper. Ensuring stable control of EMS maglev suspension systems is critical for operational safety [6–8]. Accordingly, research in this field has evolved from linear and nonlinear control methods to contemporary artificial intelligence techniques [9–12].

Among these control algorithms, sliding mode control (SMC) is widely adopted due to its inherent robustness against model inaccuracies, parameter uncertainties, and external disturbances [13–16]. When the system state reaches the sliding manifold, its dynamics become exclusively determined by the predefined sliding surface [17, 18]. The core question emerges: What type of controller should we design to ensure system variables reach the sliding manifold within the desired time frame? Finite-time

stability (FTS) enables fast convergence but with initial-state-dependent settling time [19–22]. Fixed-time stability (FXTS) removes initial-state dependence while remaining parameter-sensitive [23–27]. Prespecified-time stability (PSTS) represents a significant advancement by offering a user-defined convergence time completely independent of both initial states and system parameters, a crucial feature for high-precision applications [28–32].

While PSTS has demonstrated promising results in spacecraft attitude control and neural network synchronization, its application to maglev systems remains largely unexplored. Successful implementation would provide two critical benefits: (i) guaranteed convergence within operator-specified timeframes regardless of operating conditions, and (ii) significantly enhanced reliability for high-speed maglev operation. Therefore, the proposed PSTS controller maintains robustness against electromagnetic disturbances while guaranteeing exact prespecified-time convergence. This preliminary effort seeks to modestly contribute to transportation control systems through a balanced integration of theoretical principles and practical constraints.

This paper is organized as follows. Section 2 presents the maglev system dynamics model. Section 3 develops three distinct controllers to achieve finite-time, fixed-time, and prespecified-time stability on the sliding surface. Section 4 conducts numerical simulations to validate the effectiveness of the proposed control strategies. Finally, Section 5 concludes the paper.

2. The maglev system model

Figure 1 shows the schematic diagram of a single-degree-of-freedom suspension system as in [3,33].

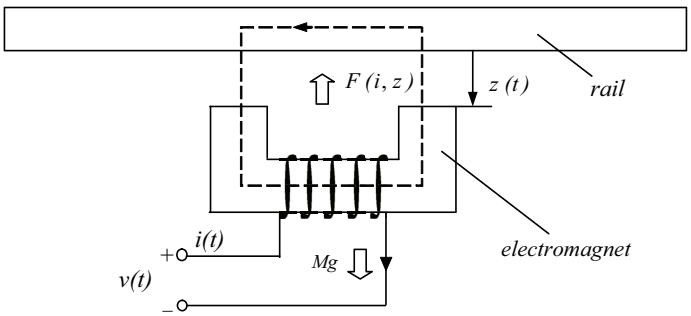

Figure 1. The schematic diagram of a single-degree-of-freedom suspension system.

Its corresponding dynamics can be mathematically modeled as follows:

$$\begin{aligned} &m\ddot{z}(t) = mg - F(i,z), \\ &F(i,z) = \frac{\mu_0 N^2 S_0}{4}\left[\frac{i(t)}{z(t)}\right]^2, \\ &u(t) = ri(t) + \frac{\mu_0 N^2 S_0}{2}\frac{\dot{i}(t)}{z(t)} - \frac{\mu_0 N^2 S_0 i(t)}{2}\frac{\dot{z}(t)}{[z(t)]^2}, \end{aligned} \tag{2.1}$$

where the variable $z(t)$ represents the absolute vertical displacement of the electromagnet, which corresponds to the suspension gap. The terms $F(i,z)$ and mg denote the electromagnetic force and

the weight of the electromagnet, respectively. The time-dependent variables $i(t)$ and $u(t)$ represent the current and voltage of the electromagnet winding, respectively. Additionally, μ_0, N, and S_0 denote the magnetic permeability of free space, the number of coil turns, and the pole area, respectively. Finally, r represents the resistance of the electromagnet.

For simplicity, let $k = \frac{1}{4}N^2\mu_0 S_0$. Define the variable $(z, \dot{z}, i/z, (i/z)')^T$, the variable i/z represents the electromotive force of the electromagnet winding, which corresponds to a physically measureable quantity. According to (2.1), the values of the state variables at the balance point are $(z_e, 0, \sqrt{mg/k}, 0)$, where z_e is a nominal value of the air gap z. Moving the equilibrium to the origin, letting $X = (x_1, x_2, x_3, x_4)^{\mathrm{T}} = (z - z_e, \dot{z}, i/z - \sqrt{mg/k}, (i/z)')^{\mathrm{T}}$, (2.1) becomes

$$\begin{aligned} \dot{x_1} &= x_2, \\ \dot{x_2} &= -\frac{kx_3^2}{m} - 2\sqrt{\frac{kg}{m}}x_3, \\ \dot{x_3} &= x_4, \\ \dot{x_4} &= -\frac{r}{2k}(x_1 + z_e)(x_3 + \sqrt{\frac{mg}{k}}) + \frac{1}{2k}u, \end{aligned} \tag{2.2}$$

where u is the control voltage applied to the electromagnet to stabilize the suspension beneath the guideway, as the open-loop electromagnetic suspension system is inherently unstable.

3. Sliding mode control design

In this section, we propose an overall sliding mode control (SMC) scheme for the maglev system. The control design consists of two independent components: ensuring global stability of the motion on the sliding surface, and deriving a controller to achieve finite-time convergence to the surface. To simplify notation, denote $f_1 = -\frac{kx_3^2}{m} - 2\sqrt{\frac{kg}{m}}x_3$, $f_2 = -\frac{r}{2k}(x_1 + z_e)(x_3 + \sqrt{\frac{mg}{k}})$. Then, the error variables are defined as

$$\begin{aligned} e_1 &= x_1, \\ e_2 &= x_2, \\ e_3 &= f_1 = -\frac{kx_3^2}{m} - 2\sqrt{\frac{kg}{m}}x_3, \\ e_4 &= \dot{f_1} = -2(\frac{kx_3}{m} + \sqrt{\frac{kg}{m}})x_4, \end{aligned} \tag{3.1}$$

The corresponding error vector is $E = [e_1, e_2, e_3, e_4]^T = [e_1, \dot{e}_1, \ddot{e}_1, \dddot{e}_1]^T$. A switching surface is defined as:

$$s = c_1e_1 + c_2e_2 + c_3e_3 + e_4 \tag{3.2}$$

where c_1, c_2, and c_3 are positive constants chosen such that the polynomial

$$\lambda^3 + c_3\lambda^2 + c_2\lambda + c_1 \tag{3.3}$$

is Hurwitz (i.e., all its roots have negative real parts). This ensures that the error dynamics in sliding mode are asymptotically stable. Next, a control law is derived to enforce the sliding condition $s \to 0$, ensuring the stability of the maglev system.

3.1. Finite-time stability

Lemma 1 [34] **(Finite-time stability):** Suppose $V(\cdot) : R^n \to R_+ \cup 0$ is $C-$regular and $x(t) \in R^n$ is absolutely continuous on any compact subinterval of $[0, +\infty]$. If $V(x(t))$ satisfies

$$\dot{V}(x(t)) \leq -\beta V^{\eta}(x(t)), \forall t \geq 0, \tag{3.4}$$

where $\beta > 0, 0 < \eta < 1$ are two constants, then we have $V(x(t)) \equiv 0, \forall t \geq T_n$, and the settling time T_n is given by

$$T_n = \frac{V^{1-\eta}(x(0))}{\beta(1-\eta)}. \tag{3.5}$$

The sliding mode control comprises two distinct components: an equivalent control term u_{eq} derived from the system dynamics on the sliding surface $s = 0$, obtained by solving $\dot{s} = 0$, and a switching control term u_{sw} that ensures reachability of the sliding surface as.

$$u_{eq} = -(\frac{1}{2k}\frac{df_1}{dx_3})^{-1}(c_1x_2 + c_2f_1 + c_3\frac{df_1}{dx_3}x_4 + \frac{d}{dt}(\frac{df_1}{dx_3})x_4 + \frac{df_1}{dx_3}f_2) \tag{3.6}$$

$$u_{sw1} = -(\frac{1}{2k}\frac{df_1}{dx_3})^{-1} \cdot \beta \text{sign}(s), \tag{3.7}$$

where $\beta > 0$.

The sliding mode controller is

$$u_1 = u_{eq} + u_{sw1}. \tag{3.8}$$

Theorem 1: The variables (3.1) with the control law (3.8) have uniform FNTC systems. And, the settling time of the closed-loop system is given as

$$T_n = \frac{\sqrt{2}V^{\frac{1}{2}}(x(0))}{\beta}. \tag{3.9}$$

Proof. Consider the Lyapunov function candidate:

$$V = \frac{1}{2}s^2.$$

Taking its time derivative yields

$$\dot{V} = s\dot{s}.$$

Recall that $f_1 = -\frac{kx_3^2}{m} - 2\sqrt{\frac{kg}{m}}x_3$. Then,

$$\dot{f_1} = \frac{df_1}{dx_3} \cdot \dot{x}_3 = \frac{df_1}{dx_3}x_4,$$

where

$$\frac{df_1}{dx_3} = -\frac{2kx_3}{m} - 2\sqrt{\frac{kg}{m}}.$$

Taking the second derivative,

$$\ddot{f}_1 = \frac{d}{dt}\left(\frac{df_1}{dx_3}\right)x_4 + \frac{df_1}{dx_3}\dot{x}_4.$$

From the system dynamics, we have $\dot{x}_4 = f_2 + \frac{1}{2k}u$, where f_2 represents the remaining system dynamics. Therefore,

$$\ddot{f}_1 = \frac{d}{dt}\left(\frac{df_1}{dx_3}\right)x_4 + \frac{df_1}{dx_3}\left(f_2 + \frac{1}{2k}u\right).$$

Then,

$$\begin{aligned}
\dot{s} &= c_1x_2 + c_2f_1 + c_3\frac{df_1}{dx_3}x_4 + \frac{d}{dt}\left(\frac{df_1}{dx_3}\right)x_4 + \frac{df_1}{dx_3}f_2 + \frac{df_1}{dx_3}\cdot\frac{1}{2k}u \\
&= c_1x_2 + c_2f_1 + c_3\frac{df_1}{dx_3}x_4 + \frac{d}{dt}\left(\frac{df_1}{dx_3}\right)x_4 + \frac{df_1}{dx_3}f_2 + \frac{df_1}{dx_3}\cdot\frac{1}{2k}(u_{eq} + u_{sw1}) \\
&= c_1x_2 + c_2f_1 + c_3\frac{df_1}{dx_3}x_4 + \frac{d}{dt}\left(\frac{df_1}{dx_3}\right)x_4 + \frac{df_1}{dx_3}f_2 \\
&\quad + \frac{df_1}{dx_3}\cdot\frac{1}{2k}\left[-\left(\frac{1}{2k}\frac{df_1}{dx_3}\right)^{-1}\left(c_1x_2 + c_2f_1 + c_3\frac{df_1}{dx_3}x_4 + \frac{d}{dt}\left(\frac{df_1}{dx_3}\right)x_4 + \frac{df_1}{dx_3}f_2\right) + u_{sw1}\right] \\
&= c_1x_2 + c_2f_1 + c_3\frac{df_1}{dx_3}x_4 + \frac{d}{dt}\left(\frac{df_1}{dx_3}\right)x_4 + \frac{df_1}{dx_3}f_2 \\
&\quad - \left(c_1x_2 + c_2f_1 + c_3\frac{df_1}{dx_3}x_4 + \frac{d}{dt}\left(\frac{df_1}{dx_3}\right)x_4 + \frac{df_1}{dx_3}f_2\right) + \frac{df_1}{dx_3}\cdot\frac{1}{2k}u_{sw1} \\
&= \frac{df_1}{dx_3}\cdot\frac{1}{2k}u_{sw1} \\
&= \frac{df_1}{dx_3}\cdot\frac{1}{2k}\left[-\left(\frac{1}{2k}\frac{df_1}{dx_3}\right)^{-1}\beta\text{sign}(s)\right] \\
&= -\beta\text{sign}(s).
\end{aligned}$$

Therefore, the time derivative of the Lyapunov function becomes:

$$\dot{V} = s\dot{s} = s\left(-\beta\text{sign}(s)\right) = -\beta|s|.$$

Since $V = \frac{1}{2}s^2$, we have $|s| = \sqrt{2V}$, thus:

$$\dot{V} = -\beta\sqrt{2V} = -\beta\sqrt{2}V^{1/2}.$$

Let $\beta' = \beta\sqrt{2}$. Then,

$$\dot{V} = -\beta' V^{1/2}.$$

According to Lemma 1 (finite-time stability), with $\eta = \frac{1}{2}$ and $\beta = \beta'$, the system reaches the sliding surface $s = 0$ in finite time. The settling time is estimated as:

$$T_n = \frac{V^{1-\eta}(x(0))}{\beta'(1-\eta)} = \frac{V^{1/2}(x(0))}{\beta'\cdot(1/2)} = \frac{2V^{1/2}(x(0))}{\beta\sqrt{2}} = \frac{\sqrt{2}V^{1/2}(x(0))}{\beta}.$$

3.2. Fixed-time stability

Lemma 2 [23] **(Fixed-time stability):** Let $V(\cdot): R^n \to R_+ \cup 0$ be a continuous radically unbounded function. Suppose the following two conditions hold:

(i) $V(x(t)) = 0 \leftrightarrow x(t) = 0$;

(ii) $\dot{V}(x(t)) \leq -aV^p(x(t)) - bV^q(x(t))$, for some $a, b > 0, 0 < p < 1$ and $q > 1$.

Then, the origin of the system is fixed-time stable, and the settling time of the closed-loop system is given as

$$T_x = \frac{1}{a(1-p)} + \frac{1}{b(q-1)}. \tag{3.10}$$

The switching control term is designed as follows

$$u_{sw2} = -(\frac{1}{2k}\frac{df_1}{dx_3})^{-1}(a\text{sign}(s) \mid s \mid^p + b\text{sign}(s) \mid s \mid^q) \tag{3.11}$$

where $a, b > 0, 0 < p < 1$, and $q > 1$. The proposed state feedback control law is

$$u_2 = u_{eq} + u_{sw2} \tag{3.12}$$

Theorem 2: The variables (3.1) with the control law (3.13) are fixed-time stable, and the settling time of the closed-loop system is given as

$$T_x = \frac{1}{a \cdot 2^{\frac{p-1}{2}}(1-p)} + \frac{1}{b \cdot 2^{\frac{q-1}{2}}(q-1)}. \tag{3.13}$$

Proof. Consider the Lyapunov function candidate:

$$V = s^2/2,$$

taking its time derivative and substituting the system dynamics (3.2) with control law (3.13) yields,

$$\begin{aligned}
\dot{V} &= s\dot{s} = s(c_1\dot{e}_1 + c_2\dot{e}_2 + c_3\dot{e}_3 + \dot{e}_4) \\
&= s[c_1x_2 + c_2f_1 + c_3\frac{df_1}{dx_3}x_4 + \frac{\mathrm{d}}{\mathrm{dt}}(\frac{df_1}{dx_3})x_4 + \frac{df_1}{dx_3}(f_2 + \frac{1}{2k}u)] \\
&\leq -a \mid s \mid^{p+1} - b \mid s \mid^{q+1} \\
&= -a(\frac{1}{2}s^2)^{\frac{p+1}{2}} \cdot 2^{\frac{p+1}{2}} - b(\frac{1}{2}s^2)^{\frac{q+1}{2}} \cdot 2^{\frac{q+1}{2}} \\
&= -a \cdot 2^{\frac{p+1}{2}} \cdot V^{\frac{p+1}{2}} - b \cdot 2^{\frac{q+1}{2}} \cdot V^{\frac{q+1}{2}}.
\end{aligned} \tag{3.14}$$

Since $0 < p < 1$ and $q > 1$, then $\frac{p+1}{2} > 1, 0 < \frac{q+1}{2} < 1$. According to Lemma 2, the error system (3.1) achieves the switching surface (3.2) under controller (3.13), ensuring fixed-time convergence. From (3.9), the settling time estimate is given by

$$T_x = \frac{1}{a \cdot 2^{\frac{p-1}{2}}(1-p)} + \frac{1}{b \cdot 2^{\frac{q-1}{2}}(q-1)}.$$

3.3. Prespecified-time stability

Lemma 3 [35] **(Prespecified-time stability):** Suppose $T_p > 0$ is a prespecified-time, and the constant $0 < \rho < 1$. If the Lyapunov function $V : R^n \to R$ possesses C-regularity and satisfies

$$\frac{dV}{dt} \leq -\frac{T_x}{T_p}(1 + V^{2\rho})V^{1-\rho}, \tag{3.15}$$

for a.e. $t \geq 0$, then the origin of the system is prespecified-time stable, where the actual expression for T_x is in (3.9). The switching control term is designed as follows:

$$u_{sw3} = -(\frac{1}{2k}\frac{df_1}{dx_3})^{-1}(\frac{1}{T_p}\psi(s)\cdot \mid s \mid^{1-\rho} \cdot \text{sign}(s)) \tag{3.16}$$

where $\psi(s) = T_x \cdot (1 + (\frac{1}{2}s^2)^\rho)$. The proposed state feedback control law is

$$u_3 = u_{eq} + u_{sw3}. \tag{3.17}$$

Theorem 3: The variables (3.1) with the control law (3.18) are prespecified-time stable, and the settling time of the closed-loop system is T_p.

Proof. Consider the Lyapunov function candidate:

$$V = s^2/2,$$

taking its time derivative and substituting the system dynamics (3.2) with control law (3.18) yields,

$$\begin{aligned}
\dot{V} = s\dot{s} &= s(c_1\dot{e}_1 + c_2\dot{e}_2 + c_3\dot{e}_3 + \dot{e}_4) \\
&= s[c_1x_2 + c_2f_1 + c_3\frac{df_1}{dx_3}x_4 + \frac{\mathrm{d}}{\mathrm{dt}}(\frac{df_1}{dx_3})x_4 + \frac{df_1}{dx_3}(f_2 + \frac{1}{2k}u)] \\
&\leq -\frac{1}{T_p}\psi(s)\cdot \mid s \mid^{2-\rho} \\
&= -\frac{T_x}{T_p}(1 + (\frac{1}{2}s^2)^\rho) \cdot (s^2)^{1-\frac{\rho}{2}} \\
&= -\frac{T_x}{T_p}(1 + V^\rho) \cdot V^{1-\frac{\rho}{2}}.
\end{aligned} \tag{3.18}$$

Since $0 < \rho < 1$, then $0 < \frac{\rho}{2} < 1$. According to Lemma 3, the variables (3.1) achieve the switching surface (3.2) under controller (3.18), ensuring prespecified-time convergence, and the settling time is T_p.

Theorems 1–3 demonstrate that the variables (3.1) achieve finite-time, fixed-time, and prespecified-time convergence to the sliding surface under their respective controllers. Since c_1, c_2, and c_3 are chosen as positive constants ensuring the polynomial $\lambda^3 + c_3\lambda^2 + c_2\lambda + c_1$ is Hurwitz, the error variables e_1, e_2, and e_3 will globally converge to zero from any initial conditions. On the ideal sliding mode$s = 0$, where $e_4 = -c_1e_1 - c_2e_2 - c_3e_3$, the error variable e_4 will consequently also converge to zero. Next, we demonstrate that the vector $X = [x_1, x_2, x_3, x_4]^{\mathrm{T}}$ converges to zero as $E \to 0$. From (3.2), it follows

that $e_1 = x_1, e_2 = x_2$, and $e_3 = f_1$ are stabilized. In practical applications, both the current I and the air gap z must remain positive. Consequently, I/z is inherently positive. This implies that x_3 (given by $I/z - \sqrt{mg/k}$) in Eq (3.1) must satisfy $x_3 \geq -\sqrt{mg/k}$. Given the stability of e_3, where

$$e_3 = f_1 = -\frac{kx_3^2}{m} - 2\sqrt{\frac{kg}{m}}x_3,$$

it follows that must x_3 converge to zero. Similarly, x_4 converges to zero once e_4 is stabilized.

Thus, under the controllers (3.8), (3.13), and (3.18), all state variables of system (2.2) asymptotically converge to the equilibrium point.

3.4. Singularity analysis

The control laws in Eqs (3.8), (3.12), and (3.17) involve a term $\frac{1}{2k}\frac{df_1}{dx_3}$ in the denominator. A potential singularity occurs when $\frac{df_1}{dx_3} = 0$, which would lead to an unbounded control input. From (3.1), we have

$$\frac{df_1}{dx_3} = -\frac{2k}{m}x_3 - 2\sqrt{\frac{kg}{m}}. \tag{3.19}$$

Setting Eq (3.19) to zero yields:

$$x_3 = -\sqrt{\frac{mg}{k}}. \tag{3.20}$$

Recall that $x_3 = i/z - \sqrt{mg/k}$. Hence, the condition $\frac{df_1}{dx_3} = 0$ corresponds to $i/z = 0$, which is physically infeasible in a maglev system because it would imply zero electromagnetic force. Moreover, the equilibrium point of the system is at $x_3 = 0$ (i.e., $i/z = \sqrt{mg/k}$). Therefore, the singularity condition in Eq (3.20) is *not* within the operational region of interest. In fact, for the system to be in a stable levitation state, we require x_3 to be around zero. It is straightforward to verify that at the equilibrium, $\frac{df_1}{dx_3} = -2\sqrt{\frac{kg}{m}} \neq 0$. Furthermore, during operation, the state x_3 is expected to deviate only within a small neighborhood of the equilibrium, ensuring that $\frac{df_1}{dx_3}$ remains bounded away from zero.

Remark 1. The proposed PSTS scheme guarantees prespecified-time stability, where the settling time T_p is a direct tunable parameter, enabling precise convergence control. Unlike finite/fixed-time methods, its convergence time is independent of system parameters and initial conditions, ensuring predictable performance under varying operations. As a practical extension of fixed-time theory, PSTS offers a direct framework for time-constrained control, particularly valuable for systems like maglev that require explicit settling-time guarantees, thereby enhancing both design transparency and practical utility.

Remark 2. The sliding mode controller designed in this study directly outputs the coil terminal voltage u, based on the full system model (2.1) that includes electromagnetic dynamics. In practical implementation, a common improvement is to adopt a current tracking architecture. Specifically, the equivalent force command from the controller can be converted into a desired current through the force current relationship, and an inner loop current controller (e.g., a PID controller) can be added to drive the power amplifier. However, since the main aim of this paper is to verify the stability and robustness of the proposed sliding mode algorithm under the complete nonlinear model, all simulations and comparisons are kept within the same voltage control framework to simplify the analysis and focus on the key issues.

4. Numerical simulation

In our analysis, we adopt the physical parameters of the Changsha low-speed magnetic levitation system (Table 1) to develop the maglev dynamic model.

Table 1. Physical parameter values.

Parameter	Symbol	Value
Number of turns	N	320
Wire radius	r	0.5 Ω
Mass	m	500 kg
Permeability of free space	μ_0	$4\pi \times 10^{-7}$
Equilibrium displacement	z_e	0.008 m
Cross-sectional area	S_0	0.047 m^2

The corresponding value of k can be derived: $k = \frac{1}{4}N^2\mu_0 S_0 = 0.0015$. The initial condition $x(0) = (0.001, 0.05, 0.002, 0.003)^T$ and time interval is $t = 0.001$. $c1, c2$, and $c3$ are often chosen such that the three order polynomial has a pair of conjugate complex roots with negative real parts and a negative real root. When $c_1 = 21.75, c_2 = 22.25$, and $c_3 = 8$, the roots of the characteristic polynomial are $-2.5 \pm 1i$ and -3.

We conducted numerical simulations based on Theorems 1–3, employing Controllers (3.8), (3.13), and (3.18), respectively, using the physical data from Table 1 and the parameter values mentioned above. Here, we only present the responses of the two state variables of greatest concern in engineering applications: the suspension gap x_1 and the state variable x_3.

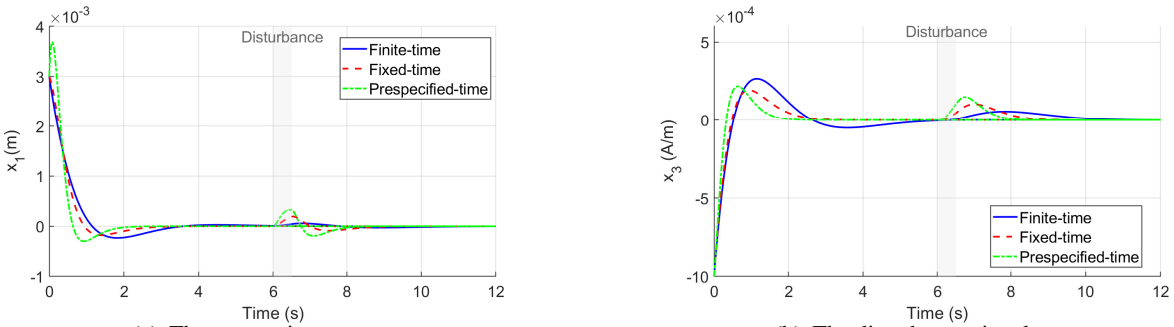

(a) The suspension gap x_1 (b) The disturbance signal $\triangle x_1$

Figure 2. Comparison of the suspension gap x_1 under different controllers.

Under the action of Controller (3.8), these two states achieve stability in finite time, with a settling time of approximately $t \approx 5.9s$ (as indicated by the dashed lines in Figures 2(a),(b)). Subsequently, Controller (3.13) is adopted to achieve stability in fixed time. From Eq (3.11), selecting $a = b = 0.8, p = 0.5$, and $q = 2$ yields a calculated settling time of $T_x \approx 3.856s$, which is essentially consistent with the simulation results (as shown by the solid lines in Figures 2(a),(b)). Finally, Controller (3.18) is employed to achieve prespecified-time stability. Based on the aforementioned $T_x \approx 3.856$, we set $T_p = 3s, \rho = 0.5$. The two states stabilize within approximately 3 s (as depicted by the dotted lines

in Figures 2(a),(b)), which is close to the preset time T_p. The slight deviation is attributed to practical limitations such as actuator saturation and system noise, as expected in real-world implementations.

The comparative responses under a 10% rated load disturbance (490 N, applied at $t = 6s$ for $0.5s$ duration, indicated by the gray shaded region) are presented. A random disturbance (band-limited white noise, 0.8 Hz cutoff) is applied to state x_1 to simulate noise. The responses of three controllers are compared under the same disturbance (see Figure 3).

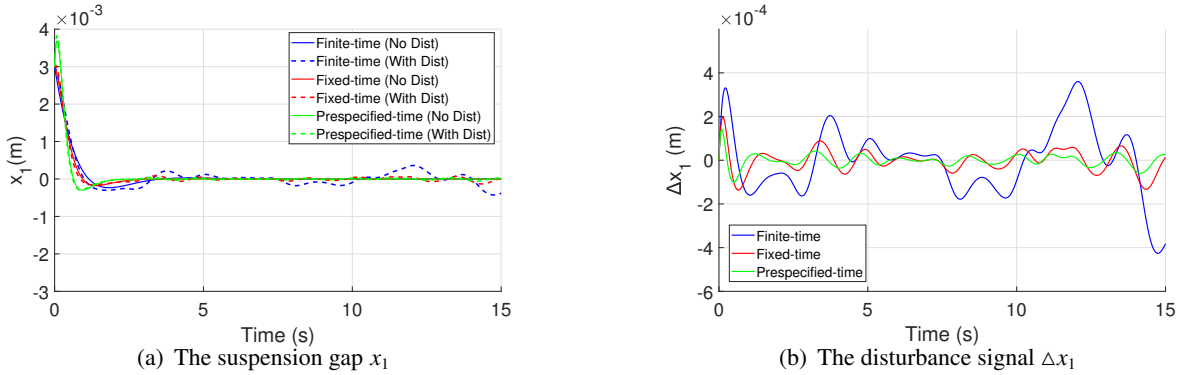

(a) The suspension gap x_1 (b) The disturbance signal $\triangle x_1$

Figure 3. Comparison of the suspension gap x_1 under different controllers.

Both figures demonstrate that the prespecified-time controller achieves superior disturbance attenuation with minimal state deviations and fastest recovery to equilibrium, while the fixed-time and finite-time controllers exhibit larger oscillations and slower settling. The results confirm the enhanced robustness of prespecified-time control against external disturbances in the magnetic levitation system.

5. Conclusions

This paper has systematically addressed the prespecified-time stability problem for maglev train suspension systems through a sliding mode control approach. Three novel controllers were developed to achieve finite-time, fixed-time, and prespecified-time stability, respectively. The control design involved the construction of appropriate sliding manifolds and the application of pole assignment techniques to precisely regulate system dynamics on the sliding surface. Stability of each controller was rigorously verified using Lyapunov analysis. Numerical simulations, conducted under realistic maglev suspension system parameters, demonstrated that the proposed controllers effectively achieved their respective stability objectives. The prespecified-time controller notably enabled exact convergence within a user-defined time T_p, showing superior precision and practical applicability. The methods presented in this work offer a theoretical foundation and practical framework for high-performance maglev suspension control, with significant potential for enhancing safety, comfort, and reliability in high-speed transportation systems.

Use of AI tools declaration

The authors declare they have not used Artificial Intelligence (AI) tools in the creation of this article.

Acknowledgments

Scientific Research Fund of Hunan Provincial Education Department of China, Grant/Award Number: 24A0633, the National Natural Science Foundation of China, No.12171056 (L. Huang).

Conflict of interest

The authors declare there are no conflicts of interest.

References

1. Q. Zhu, S. M. Wang, Y. Q. Ni, A review of levitation control methods for low-and medium-speed maglev systems, *Buildings*, **14** (2024), 837. https://doi.org/10.3390/buildings14030837
2. H. W. Lee, K. C. Kim, J. Lee, Review of maglev train technologies, *IEEE Trans. Magn.*, **42** (2006), 1917–1925. https://doi.org/10.1109/TMAG.2006.875842
3. L. Zhang, L. Huang, Hopf bifurcation analysis for a maglev system with two time delays, *Mech. Syst. Signal Process.*, **224** (2025), 112006. https://doi.org/10.1016/j.ymssp.2024.112006
4. S. K. Kim, C. K. Ahn, Sensorless non-linear position-stabilising control for magnetic levitation systems, *IET Control Theory Appl.*, **14** (2020), 2682–2687. https://doi.org/10.1049/iet-cta.2020.0295
5. C. Chen, J. Xu, G. Lin, Y. Sun, F. Ni, Model identification and nonlinear adaptive control of suspension system of high-speed maglev train, *Veh. Syst. Dyn.*, **60** (2022), 884–905. https://doi.org/10.1080/00423114.2020.1838564
6. F. Zhao, K. You, S. Song, W. Zhang, L. Tong, Suspension regulation of medium-low-speed maglev trains via deep reinforcement learning, *IEEE Trans. Artif. Intell.*, **2** (2021), 341–351. https://doi.org/10.1109/TAI.2021.3097313
7. Y. Sun, J. Xu, G. Lin, W. Ji, L. Wang, RBF neural network-based supervisor control for maglev vehicles on an elastic track with network time delay, *IEEE Trans. Ind. Inf.*, **18** (2020), 509–519. https://doi.org/10.1109/TII.2020.3032235
8. X. Bu, L. Wang, Y. Han, H. Liu, P. Hu, C. Cai, Dynamic model of high-speed maglev train-guideway bridge system with a nonlinear suspension controller, *Adv. Struct. Eng.*, **27** (2024), 1328–1348. https://doi.org/10.1177/13694332241247921
9. B. Bidikli, An observer-based adaptive control design for the maglev system, *Trans. Inst. Meas. Control*, **42** (2020), 2771–2786. https://doi.org/10.1177/0142331220932396
10. Y. Sun, J. Xu, G. Lin, N. Sun, Adaptive neural network control for maglev vehicle systems with time-varying mass and external disturbance, *Neural Comput. Appl.*, **35** (2023), 12361–12372. https://doi.org/10.1007/s00521-021-05874-2
11. H. Qiang, C. Xiao, H. Huang, Y. Hai, Y. Sun, Yaw feedback control of active steering vehicle based on differential flatness theory, *J. Theor. Appl. Mech.*, **63** (2025), 131–149. https://doi.org/10.15632/jtam-pl/195727

12. Z. Zhang, Y. Pan, W. Zhao, J. Zhang, Z. Zi, Y. Xie, et al., Frequency analysis of a discrete - time fast nonlinear tracking differentiator algorithm based on isochronic region method, *Electron. Res. Arch.*, **32** (2024), 5157–5175. https://doi.org/10.3934/era.2024238
13. R. Xu, U. Özgüner, Sliding mode control of a class of underactuated systems, *Automatica*, **44** (2008), 233–241. https://doi.org/10.1016/j.automatica.2007.05.014
14. L. Zhang, Z. Zhang, Z. Long, A. Hao, Sliding mode control with auto-tuning law for maglev system, *Engineering*, **2** (2010), 107–112. https://doi.org/10.4236/eng.2010.22015
15. C. Lei, Y. Lan, Z. Xu, Y. Sun, Fixed-time dual sliding mode control for linear synchronous motor maglev systems, *Int. J. Robust Nonlinear Control*, **34** (2024), 3781–3797. https://doi.org/10.1002/rnc.7162
16. Y. Liu, Y. Zhang, Y. Kao, Z. Gao, Sliding mode control for delta operator sampled systems, *IEEE Trans. Autom. Sci. Eng.*, **22** (2025), 8006–8017. https://doi.org/10.1109/TASE.2024.3476085
17. Y. Gai, M. Chen, H. Wang, L. Wu, K. Peng, Fixed-time tracking control of quadrotor UAVs based on disturbance observer and sliding mode, *Int. J. Syst. Sci.*, **57** (2026), 647–667. https://doi.org/10.1080/00207721.2025.2505714
18. F. Bayat, M. Javaheri, Two-layer terminal sliding mode attitude control of satellites equipped with reaction wheels, *Asian J. Control*, **22** (2020), 388–397. https://doi.org/10.1002/asjc.1878
19. S. P. Bhat, D. S. Bernstein, Finite-time stability of continuous autonomous systems, *SIAM J. Control Optim.*, **38** (2000), 751–766. https://doi.org/10.1137/S0363012997321358
20. E. Moulay, W. Perruquetti, Finite time stability of differential inclusions, *IMA J. Math. Control Inf.*, **22** (2005), 465–475. https://doi.org/10.1093/imamci/dni039
21. Y. Orlov, Finite time stability and robust control synthesis of uncertain switched systems, *SIAM J. Control Optim.*, **43** (2005), 1253–1271. https://doi.org/10.1137/S0363012903425593
22. M. Forti, M. Grazzini, P. Nistri, L. Pancioni, Generalized Lyapunov approach for convergence of neural networks with discontinuous or non-Lipschitz activations, *Physica D*, **214** (2006), 88–99. https://doi.org/10.1016/j.physd.2005.12.006
23. A. Polyakov, Nonlinear feedback design for fixed-time stabilization of linear control systems, *IEEE Trans. Autom. Control*, **57** (2012), 2106–2110. https://doi.org/10.1109/TAC.2011.2179869
24. A. Polyakov, D. Efimov, W. Perruquetti, Finite-time and fixed-time stabilization: implicit Lyapunov function approach, *Automatica*, **51** (2015), 332–340. https://doi.org/10.1016/j.automatica.2014.10.082
25. F. Lopez-Ramirez, D. Efimov, A. Polyakov, W. Perruquetti, Conditions for fixed-time stability and stabilization of continuous autonomous systems, *Syst. Control Lett.*, **129** (2019), 26–35. https://doi.org/10.1016/j.sysconle.2019.05.003
26. C. Chen, L. X. Li, H. P. Peng, Y. Yang, L. Mi, H. Zhao, A new fixed-time stability theorem and its application to the fixed-time synchronization of neural networks, *Neural Networks*, **123** (2020), 412–419. https://doi.org/10.1016/j.neunet.2019.12.028
27. Z. W. Cai, L. H. Huang, Z. Y. Wang, Finite-/fixed-time stability of nonautonomous functional differential inclusion: Lyapunov approach involving indefinite derivative, *IEEE Trans. Neural Networks Learn. Syst.*, **33** (2022), 6763–6774. https://doi.org/10.1109/TNNLS.2021.3083396

28. C. D. Liang, M. F. Ge, Z. W. Liu, X. Zhang, J. H. Park, Predefined-time stabilization of T-S fuzzy systems: a novel integral sliding mode-based approach, *IEEE Trans. Fuzzy Syst.*, **30** (2022), 4423–4433. https://doi.org/10.1109/TFUZZ.2022.3152834

29. Y. H. Ren, W. N. Zhou, Z. W. Li, Y. Q. Sun, Prescribed-time consensus tracking of multiagent systems with nonlinear dynamics satisfying time-varying Lipschitz growth rates, *IEEE Trans. Cybern.*, **53** (2023), 2097–2109. https://doi.org/10.1109/TCYB.2021.3109294

30. F. C. Kong, H. L. Ni, Q. X. Zhu, C. Hu, T. Huang, Fixed-time and predefined-time synchronization of discontinuous neutral-type competitive networks via non-chattering adaptive control strategy, *IEEE Trans. Network Sci. Eng.*, **10** (2023), 3644–3657. https://doi.org/10.1109/TNSE.2023.3271109

31. S. Z. Xie, Q. Chen, Predefined-time disturbance estimation and attitude control for rigid spacecraft, *IEEE Trans. Circuits Syst. II Express Briefs*, **71** (2024), 2089–2093. https://doi.org/10.1109/TCSII.2023.3331825

32. J. Liu, F. Yang, M. Zhang, Distributed dual-mode energy management for AC microgrids via prespecified-time dynamic event-triggered approach, *IEEE Trans. Smart Grid*, **17** (2026), 363–374. https://doi.org/10.1109/TSG.2025.3610227

33. L. Zhang, J. C. Ji, One-to-three resonant Hopf bifurcations of a maglev system, *Nonlinear Dyn.*, **93** (2018), 1277–1286. https://doi.org/10.1007/s11071-018-4258-2

34. Y. Tang, Terminal sliding mode control for rigid robots, *Automatica*, **34** (1998), 51–56. https://doi.org/10.1016/S0005-1098(97)00174-X

35. Z. Cai, L. Huang, Z. Wang, Prespecified-time control of switched neural networks: novel Lyapunov approach of prespecified-time stability, *Comput. Appl. Math.*, **43** (2024), 224. https://doi.org/10.1007/s40314-024-02748-w

AIMS Press